



1 **Seasonal variation of aerosol iron solubility in coarse and fine particles at an inland**  
2 **city in northwestern China**

3

4 Huanhuan Zhang,<sup>1,2</sup> Rui Li,<sup>1</sup> Chengpeng Huang,<sup>3</sup> Xiaofei Li,<sup>4</sup> Shuwei Dong,<sup>1</sup> Fu Wang,<sup>3</sup>  
5 Tingting Li,<sup>1</sup> Yizhu Chen,<sup>1</sup> Guohua Zhang,<sup>1</sup> Yan Ren,<sup>3</sup> Qingcai Chen,<sup>4</sup> Ru-jin Huang,<sup>5</sup> Siyu  
6 Chen,<sup>6</sup> Tao Xue,<sup>7</sup> Xinming Wang,<sup>1</sup> Mingjin Tang<sup>1,2,\*</sup>

7

8 <sup>1</sup> State Key Laboratory of Organic Geochemistry, Guangdong Key Laboratory of  
9 Environmental Protection and Resources Utilization, and Guangdong-Hong Kong-Macao Joint  
10 Laboratory for Environmental Pollution and Control, Guangzhou Institute of Geochemistry,  
11 Chinese Academy of Sciences, Guangzhou, China

12 <sup>2</sup> College of Earth and Planetary Sciences, University of Chinese Academy of Sciences, Beijing,  
13 China

14 <sup>3</sup> Longhua Center for Disease Control and Prevention of Shenzhen, Shenzhen, China

15 <sup>4</sup> School of Environmental Science and Engineering, Shaanxi University of Science and  
16 Technology, Xi'an, China

17 <sup>5</sup> State Key Laboratory of Loess and Quaternary Geology, Institute of Earth Environment,  
18 Chinese Academy of Sciences, Xi'an, China

19 <sup>6</sup> College of Atmospheric Sciences, Lanzhou University, Lanzhou, China

20 <sup>7</sup> School of Public Health, Peking University, Beijing, China

21



22 \* Correspondence: Mingjin Tang ([mingjintang@gig.ac.cn](mailto:mingjintang@gig.ac.cn))

23

24



25 **Abstract**

26 This work investigated seasonal variation of aerosol iron (Fe) solubility for coarse (>1  $\mu\text{m}$ ) and  
27 fine (<1  $\mu\text{m}$ ) particles at Xi'an, a megacity in northwestern China impacted by anthropogenic  
28 emission and desert dust. Total Fe concentrations were lowest in summer and similar in other  
29 seasons for coarse particles, while lowest in summer and highest in spring for fine particles;  
30 for comparison, dissolved Fe concentrations were higher in autumn and winter than spring and  
31 summer for coarse particles, while highest in winter and lowest in spring and summer for fine  
32 particles. Desert dust aerosol was always the major source of total Fe for both coarse and fine  
33 particles in all the four seasons, but it may not be the dominant source for dissolved Fe. Fe  
34 solubility was lowest in spring for both coarse and fine particles, and highest in winter for  
35 coarse particles and in autumn for fine particles. In general aerosol Fe solubility was found to  
36 be higher in air masses originating from local and nearby regions than those arriving from  
37 desert regions after long-distance transport. Compared to coarse particles, Fe solubility was  
38 similar for fine particles in spring but significantly higher in the other three seasons, and at a  
39 given aerosol pH range Fe solubility was always higher in fine particles. Aerosol Fe solubility  
40 was well correlated with relative abundance of aerosol acidic species, implying aerosol Fe  
41 solubility enhancement by acid processing; moreover, such correlations were better for coarse  
42 particles than fine particles in all the four seasons. Fe solubility was found to increase with  
43 relative humidity and acid acidity for both coarse and fine particles at Xi'an, underscoring the  
44 importance of aerosol liquid water and aerosol acidity in regulating Fe solubility via chemical  
45 processing.



## 46 **1 Introduction**

47       Deposition of aerosol particles is a major external source of dissolved iron (Fe) in many  
48 open oceans (Boyd and Ellwood, 2010; Tagliabue et al., 2017), significantly affecting primary  
49 production in these regions (Moore et al., 2009; Tang et al., 2021) and thus the global carbon  
50 cycle (Martin, 1990; Jickells et al., 2005). Dissolved Fe has also been recognized as an  
51 important source of reactive oxygen species in aerosol particles (Zhang et al., 2008; Fang et al.,  
52 2017; Wang et al., 2022) and thus may have adverse impacts on human health (Kelly, 2003;  
53 Abbaspour et al., 2014). In addition, dissolved Fe could catalyze aqueous oxidation of SO<sub>2</sub>  
54 (Martin and Good, 1991; Alexander et al., 2009; Huang et al., 2014), leading to the formation  
55 of sulfate, a major secondary species in aerosol particles. The various impacts of aerosol Fe are  
56 largely determined by its fractional solubility (often abbreviated as solubility) which is the ratio  
57 of dissolved Fe to total Fe.

58       Due to the impacts of dissolved aerosol Fe on ocean biogeochemistry and human health,  
59 a number of studies have been conducted in the last 2-3 decades (Mahowald et al., 2018;  
60 Meskhidze et al., 2019; Baker et al., 2021; Ito et al., 2021), leading to significant advances in  
61 our knowledge of aerosol Fe solubility and sources of aerosol dissolved Fe. For examples,  
62 many studies (Baker and Jickells, 2006; Sholkovitz et al., 2012) observed the inverse  
63 relationship between Fe solubility and total aerosol Fe. It has been recently realized that non-  
64 desert-dust sources, such as anthropogenic emissions and biomass burning, can be an important  
65 source of dissolved aerosol Fe in many regions (Sholkovitz et al., 2009; Ito et al., 2019;  
66 Hamilton et al., 2020; Liu et al., 2022), though their contribution to total aerosol Fe is usually



67 minor. Furthermore, atmospheric aging processes, such as acid processing and organic  
68 complexation, may substantially enhance solubility of Fe in desert dust and coal fly ash (Paris  
69 et al., 2011; Shi et al., 2012; Chen and Grassian, 2013; Li et al., 2017).

70 Despite significant progress, it remains difficult for modelling studies to reproduce the  
71 wide range of Fe solubility observed for ambient aerosols (Mahowald et al., 2018; Meskhidze  
72 et al., 2019). The relative contribution of non-desert-dust sources, versus desert dust, to  
73 dissolved aerosol Fe is still rather uncertain (Myriokefalitakis et al., 2018; Ito et al., 2019). In  
74 addition, the impacts of chemical processing (especially organic complexation) on aerosol Fe  
75 solubility is yet to be quantified for ambient aerosols. Further field measurements are needed  
76 to reduce the uncertainties in aerosol Fe solubility, in order to better understand the impacts of  
77 aerosol Fe on marine biogeochemistry and human health.

78 Sources, compositions and physicochemical properties are very different for coarse ( $>1$   
79  $\mu\text{m}$ ) and fine ( $<1 \mu\text{m}$ ) particles (Seinfeld and Pandis, 2016). Therefore, aerosol Fe solubility  
80 may differ significantly and is regulated by different sources or processes for coarse and fine  
81 particles, as found by previous work (Sakata et al., 2022; Zhang et al., 2022). In addition, both  
82 sources and chemical processes of aerosol particles exhibit significant variability for different  
83 seasons, consequently leading to seasonal variations in aerosol Fe solubility. As a result,  
84 examining seasonal variability of aerosol Fe solubility may provide clues for and insights into  
85 factors which regulate Fe solubility. However, seasonal variation of Fe solubility has only been  
86 explored by a few previous studies (Chen and Siefert, 2004; Tao and Murphy, 2019; Yang et  
87 al., 2020; Yang and Weber, 2022). In the present work, we investigated seasonal variations of



88 total Fe, dissolved Fe and Fe solubility for fine and coarse particles at Xi'an, a megacity in  
89 northwestern China severely affected by anthropogenic emission and desert dust (Cao and Cui,  
90 2021).

## 91 **2 Methodology**

### 92 **2.1 Sample collection**

93 Aerosol sampling in Xi'an took place during 01-30 April 2021 (spring), 12 July to 14  
94 August 2021 (summer), 07 October to 07 November (autumn) and 26 November to 31  
95 December 2020 (winter). Xi'an has a population of ~13 million and is located in the middle of  
96 the Guanzhong Plain which is surrounded by Qinling Mountains and Chinese Loess Plateau,  
97 favoring accumulation of air pollutants and formation of severe air pollution (Cao and Cui,  
98 2021). In addition, Xi'an is adjacent to major deserts in China and thus frequently affected by  
99 desert dust aerosol.

100 Sampling in winter took place at an urban site (34.23°N, 108.89°E) which is close to a  
101 busy major road and located in residential and commercial areas (Cao et al., 2012), and was  
102 carried out on a building roof (~10 m from the ground) in Institute of Earth Environment,  
103 Chinese Academy of Sciences. Sampling in the other three seasons took place at another urban  
104 site (34.37°N, 108.97°E) which is located in residential areas (Chen et al., 2021), and was  
105 carried out on a building roof (~40 m from the ground) in Shaanxi University of Science and  
106 Technology. Meteorological parameters (wind speed and direction, temperature, and relative  
107 humidity) and PM<sub>2.5</sub> and PM<sub>10</sub> mass concentrations were provided by nearby environmental  
108 monitoring stations.



109 Coarse ( $>1 \mu\text{m}$ ) and fine ( $<1 \mu\text{m}$ ) and aerosol particles were collected onto Whatman 41  
110 (W41) cellulose filters on a daily basis (from 08:00 to 07:30 next day) using a two-stage aerosol  
111 sampler (TH-150C, Tianhong Co., Wuhan, China) with a flow rate of 100 L/min. W41 filter  
112 used for aerosol sampling were acid-washed to reduce background levels. After aerosol  
113 collection, filters were sealed individually in clean plastic Petri dishes and then stored at  $-20 \text{ }^\circ\text{C}$   
114 for further analysis. Our previous work (Zhang et al., 2022) described filter pretreatment,  
115 aerosol sampling and filter storage in details. In the present work, 28, 32, 30 and 36 pairs of  
116 filter samples were collected in spring, summer, autumn and winter, respectively.

## 117 **2.2 Sample processing and analysis**

118 Sample analysis was detailed in our previous work (Zhang et al., 2022), and as a result  
119 here we only provide key information in brief. Every filter was equally cut into two halves.  
120 The first half filter, which was used to determine total Fe, was digested in a Teflon jar using  
121 microwave digestion; after residual acids used in digestion were evaporated, the Teflon jar was  
122 cooled to room temperature and then filled with 20 mL  $\text{HNO}_3$  (1%). The solution was filtered  
123 using a PTFE membrane syringe filter (pore size:  $0.22 \mu\text{m}$ ), and then analyzed using  
124 inductively coupled plasma mass spectrometry (Thermo Fisher Scientific, USA). In total 14  
125 elements were determined, including Fe, Al and Pb, and the recovery rates were found to be  
126 90-110% for Fe.

127 The other half filter, which was used to determine dissolved Fe and soluble ions, was  
128 immersed in 20 mL ultrapure water for 2 h during which an orbital shaker (300 r/min) was used  
129 to stir the aqueous mixture. After that, the aqueous mixture was filtered using a PTFE



130 membrane syringe filter (pore size: 0.22  $\mu\text{m}$ ) and then divided further to two parts. The first  
131 solution ( $\sim 10$  mL) was analyzed by ion chromatography to measure soluble anions and cations;  
132 the second solution (10 mL) was acidified to contain 1%  $\text{HNO}_3$  (using 147  $\mu\text{L}$  67%  $\text{HNO}_3$ ) and  
133 subsequently analyzed using inductively coupled plasma mass spectrometry.

### 134 **2.3 Aerosol acidity calculation**

135 The ISORROPIA-II model (Fountoukis and Nenes, 2007) was used in the “metastable +  
136 forward” mode to calculate aerosol pH for coarse and fine particles, and input data included  
137 concentrations of soluble anions ( $\text{SO}_4^{2-}$ ,  $\text{NO}_3^-$  and  $\text{Cl}^-$ ) and cations ( $\text{NH}_4^+$ ,  $\text{Na}^+$ ,  $\text{K}^+$ ,  $\text{Ca}^{2+}$  and  
138  $\text{Mg}^{2+}$ ), temperature and relative humidity (RH). The effects of  $\text{NH}_3(\text{g})$  and  $\text{HNO}_3(\text{g})$  were not  
139 taken into account as their concentrations were not measured, and this may cause some biases  
140 (likely underestimation) in calculated aerosol pH (Guo et al., 2015; Hennigan et al., 2015; Pye  
141 et al., 2020).

### 142 **2.4 Air mass back trajectory analysis**

143 The Hysplit-4 model (Draxier and Hess, 1998) was employed to calculate 48-h air mass  
144 back trajectories, using meteorological data (horizontal resolution:  $1^\circ \times 1^\circ$ ; time resolution: 6 h)  
145 from Global Data Assimilation System provided by National Centers for Environmental  
146 Prediction. Back trajectories were determined with arrival height of 100 m above the ground  
147 level and arrival time of 08:00 every day (Wang et al., 2020). In total 120, 136, 128 and 144  
148 back trajectories were obtained in our work for spring, summer, autumn and winter, and all the  
149 back trajectories were clustered using the cluster analysis method described elsewhere (Baker,  
150 2010).





### 151 **3 Total and dissolved aerosol Fe**

#### 152 **3.1 Meteorological conditions**

153 The climate in Xi'an (and the Guangzhou Plain in general) is mainly regulated by the East  
154 Asia monsoon. During our campaign, prevailing wind directions were west and southwest in  
155 spring, northeast in summer, southwest and northeast in autumn, and west in winter (Figure  
156 S1); furthermore, average wind speeds were  $>2$  m/s in summer and autumn, and  $<2$  m/s in  
157 spring and winter. Median temperatures were 13.6, 27.0, 12.7 and 1.3 °C in spring, summer,  
158 autumn and winter, and median RH were found to be 85%, 71%, 83% and 77% (Table S1).  
159 Precipitation mainly took place in summer during our campaign in 2021, similar to previous  
160 years (Cao and Cui, 2021).

161 Table S2 shows  $PM_{2.5}$  and  $PM_{10}$  concentrations at Xi'an in four seasons.  $PM_{10}$   
162 concentrations were in the range of 15-243, 24-76, 22-151 and 41-212  $\mu\text{g}/\text{m}^3$  in spring, summer,  
163 autumn and winter, and the average values were  $93\pm 6$ ,  $51\pm 16$ ,  $70\pm 35$  and  $107\pm 39$   $\mu\text{g}/\text{m}^3$ ,  
164 suggesting highest levels in spring and winter and lowest levels in summer.  $PM_{2.5}$  mass  
165 concentrations were in the range of 11-62, 11-48, 13-97 and 13-156  $\mu\text{g}/\text{m}^3$ , and the average  
166 values were  $35\pm 14$ ,  $23\pm 8$ ,  $40\pm 24$  and  $80\pm 32$   $\mu\text{g}/\text{m}^3$ , suggesting highest concentrations in winter  
167 and lowest levels in summer.

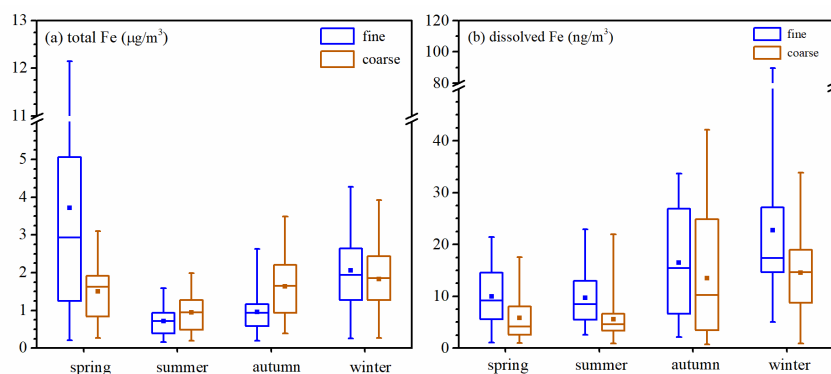
168  $PM_{2.5}$  and  $PM_{10}$  concentrations were high in winter due to accumulation of anthropogenic  
169 pollution, and the median  $PM_{2.5}/PM_{10}$  ratio was 0.76.  $PM_{10}$  concentrations in spring were  
170 significantly increased due to the impacts of desert dust aerosol, and the median  $PM_{2.5}/PM_{10}$   
171 ratio was only 0.44. Two major dust events occurred during our spring campaign (12-17 April



172 and 27-30 April). During the two dust events the average  $PM_{10}$  and  $PM_{2.5}$  mass concentrations  
173 were  $151\pm 57$  and  $42\pm 12$   $\mu\text{g}/\text{m}^3$ , and  $PM_{2.5}/PM_{10}$  ratios became even lower (0.20-0.31).  
174 Furthermore, the median  $PM_{2.5}/PM_{10}$  ratios were 0.44 in summer and 0.62 in autumn.

### 175 3.2 Total aerosol Fe

176 Figure 1a shows seasonal variation of total aerosol Fe in coarse and fine particles  
177 measured by our work at Xi'an. Total aerosol Fe concentrations were in the range of 270-3095,  
178 191-1992, 395-3492 and 269-3924  $\text{ng}/\text{m}^3$  for coarse particles in spring, summer, autumn and  
179 winter, and the average values were  $1504\pm 800$ ,  $950\pm 524$ ,  $1638\pm 830$  and  $1831\pm 866$   $\text{ng}/\text{m}^3$   
180 (Table A1); total aerosol Fe concentrations were in the range of 206-12144, 164-1591, 196-  
181 2631 and 257-4268  $\text{ng}/\text{m}^3$  for fine particles in spring, summer, autumn and winter, and the  
182 average values were  $3717\pm 3387$ ,  $721\pm 366$ ,  $958\pm 516$  and  $2058\pm 1037$   $\text{ng}/\text{m}^3$ . Average total Fe  
183 concentrations were measured to be  $798\pm 466$  and  $801\pm 534$   $\text{ng}/\text{m}^3$  for coarse and fine particles  
184 in winter (November-December 2019) at Qingdao (Zhang et al., 2022), only 44% and 38% of  
185 the average values ( $1831\pm 866$  和  $2058\pm 1037$   $\text{ng}/\text{m}^3$ ) found in winter (November-December  
186 2020) at Xi'an by the present work.



187



188 **Figure 1.** Seasonal variations of (a) total Fe and (b) dissolved Fe for fine and coarse particles.

189

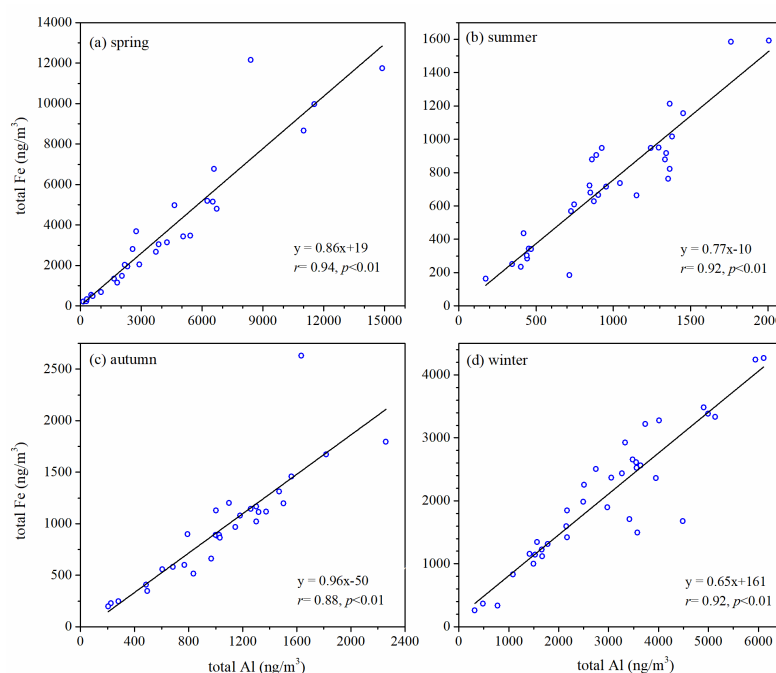
190 The average contribution of coarse particles to total Fe in TSP (total suspended particles)  
191 were 29%, 57%, 63% and 47% in spring, summer, autumn and winter. Statistical analysis  
192 (paired t-test) suggested that compared to fine particles, total Fe in coarse particles was  
193 significantly lower in spring ( $p < 0.01$ ,  $\alpha = 0.05$ ) while significantly higher in summer and autumn  
194 ( $p < 0.01$ ,  $\alpha = 0.05$ ); in addition, there was no significant difference between coarse and fine  
195 particles in winter ( $p = 0.13$ ,  $\alpha = 0.05$ ).

196 Compared to other seasons, total Fe in fine and coarse particles were both lowest in  
197 summer (Figure 1a), as aerosol mass concentrations were also lowest in summer (Section 3.1).  
198 Similarly, previous measurements on Huaniao Island in the East China Sea (Yang et al., 2020)  
199 and over the tropical and subtropical North Atlantic (Chen and Siefert, 2004) also found lowest  
200 total aerosol Fe levels in summer. For the other three seasons (spring, autumn and winter), total  
201 Fe in coarse particles were rather similar, while total Fe in fine particles were highest in spring  
202 and lowest in autumn. Overall, compared to summer and autumn, total aerosol Fe were higher  
203 in spring and winter, as the two seasons were severely affected by desert dust and  
204 anthropogenic emissions, respectively.

205 Total Fe was very well correlated with total Al ( $0.87 < r < 0.96$ ,  $p < 0.01$ ) for both coarse  
206 (Figure S3) and fine particles (Figure 2) in all the four seasons, suggesting desert dust always  
207 as the dominant source of total aerosol Fe at Xi'an, regardless of particle size range and seasons.  
208 The median [Fe]/[Al] values, mass ratios of total Fe to total Al, were 0.975, 0.926, 1.269 and



209 0.940 in spring, summer, autumn and winter for coarse particles, and 0.735, 0.796, 0.870 and  
210 0.744 for fine particles (Figure S4).  $[\text{Fe}]/[\text{Al}]$  were found to be 0.911 and 0.741 for  $\text{PM}_{10}$  and  
211  $\text{PM}_{2.5}$  generated using surface soil samples collected over several major deserts in China  
212 (Zhang et al., 2014). We found that  $[\text{Fe}]/[\text{Al}]$  measured for coarse and fine particles at Xi'an  
213 were similar to these reported for desert dust (Zhang et al., 2014); coarse particles in autumn  
214 might be one exception (Figure S4), showing slightly higher  $[\text{Fe}]/[\text{Al}]$  (median: 1.269) than  
215 desert dust.



216  
217 **Figure 2.** Total Fe versus total Al for fine particles in different seasons: (a) spring; (b) summer;  
218 (c) autumn; (d) winter.

219

### 220 3.3 Dissolved aerosol Fe



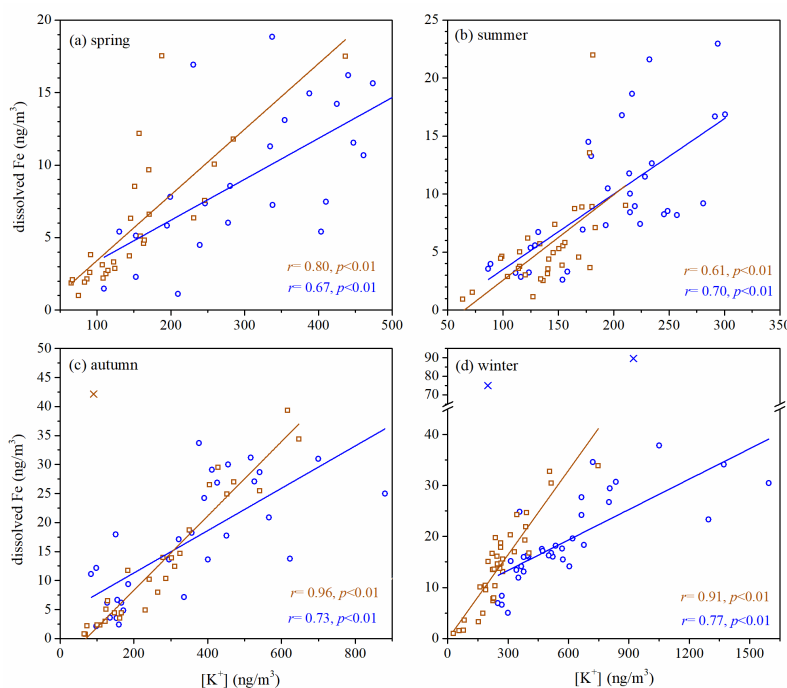
221 Figure 1b shows seasonal variation of dissolved aerosol Fe in coarse and fine particles at  
222 Xi'an. Dissolved aerosol Fe concentrations were in the range of 1.0-17.5, 0.9-22.0, 0.7-42.2  
223 and 0.9-33.8 ng/m<sup>3</sup> for coarse particles in spring, summer, autumn and winter, and the average  
224 values were 5.9±4.5, 5.6±4.0, 13.5±12.2 and 14.5±8.3 ng/m<sup>3</sup>; dissolved aerosol Fe  
225 concentrations were in the range of 1.1-21.4, 2.6-22.9, 2.1-33.7 and 5.0-89.5 ng/m<sup>3</sup> for fine  
226 particles in spring, summer, autumn and winter, and the average values were 10.0±5.5, 9.7±5.6,  
227 16.5±10.1 and 22.7±16.8 ng/m<sup>3</sup>. Average dissolved Fe concentrations were measured to be  
228 7.7±14.5 and 7.3±7.6 ng/m<sup>3</sup> for coarse and fine particles in winter at Qingdao (Zhang et al.,  
229 2022), only 53% and 32% of the average values (14.5±8.3 和 22.7±16.8 ng/m<sup>3</sup>) found in winter  
230 at Xi'an by the present work.

231 The average contribution of coarse particles to dissolved Fe in TSP were 37%, 36%, 45%  
232 and 39% in spring, summer, autumn and winter. Compared to fine particles, dissolved Fe was  
233 significantly lower in coarse particles for all the four seasons (paired t-test, p<0.01, α=0.05) at  
234 Xi'an, although total Fe in coarse particles were higher than or similar to fine particles (except  
235 spring, as discussed in Section 3.2). This indicated that aerosol Fe solubility was lower in  
236 coarse particle than fine particles, as further discussed in Section 4. Sakata et al. (2022) found  
237 that over the Pacific dissolved aerosol Fe concentrations in fine particles (<1.3 μm) were  
238 significantly higher than coarse particles (>1.3 μm).

239 Compared to spring and summer, dissolved Fe concentrations were higher in autumn and  
240 winter for coarse particles (Figure 1b); for fine particles, dissolved Fe concentrations were  
241 highest in winter, followed by autumn, and lowest in spring and summer. Dissolved Fe



242 concentrations were low in summer, as total Fe concentrations were also low (Figure 1a). Total  
243 Fe concentrations were high in spring (Figure 1a), but dissolved Fe concentrations were low;  
244 this is because compared to other seasons, spring was most severely affected by desert dust  
245 with low Fe solubility. Our previous study (Zhang et al., 2022) investigated aerosol Fe at  
246 Qingdao in winter, and found that compared to clean days, dissolved Fe concentrations did not  
247 change significantly during dust days though total Fe concentrations were remarkably  
248 increased. Therefore, our previous (Zhang et al., 2022) and current work imply that the  
249 occurrence of desert dust aerosol may not necessarily lead to increase in dissolved Fe  
250 concentrations in the air.



251

252 **Figure 3.** Dissolved Fe versus  $[K^+]$  for fine and coarse particles in different seasons: (a) spring;

253 (b) summer; (c) autumn; (d) winter.



254

255 As shown in Figure S5, overall the correlation between dissolved Fe and total Al was quite  
256 weak at Xi'an, indicating that desert dust may not contribute dominantly to dissolved aerosol  
257 Fe, although it was always the major source of total aerosol Fe (Section 3.2). We also examined  
258 correlations between dissolved Fe and several other species (Table S3). Figure 3 shows that  
259 dissolved Fe was well correlated with  $K^+$  (a tracer for biomass burning) in coarse and fine  
260 particles at all the four seasons ( $0.67 < r < 0.96$ ,  $p < 0.01$ ), and such correlation was better in  
261 autumn and winter than spring and summer. This may indicate biomass burning as an important  
262 source for dissolved aerosol Fe at Xi'an, especially in autumn and winter. Good correlation  
263 ( $0.64 < r < 0.88$ ,  $p < 0.01$ ) was also found between dissolved Fe and total Pb for coarse and fine  
264 particles except summer (Figure S6), indicating that anthropogenic emission was an important  
265 source of dissolved aerosol Fe in spring, autumn and winter. The contribution of anthropogenic  
266 emission to dissolved aerosol Fe was small in summer, partly because effective emission  
267 reduction measures were implemented during July-September 2021 at Xi'an and surrounded  
268 regions, leading to large reduction in anthropogenic emissions.

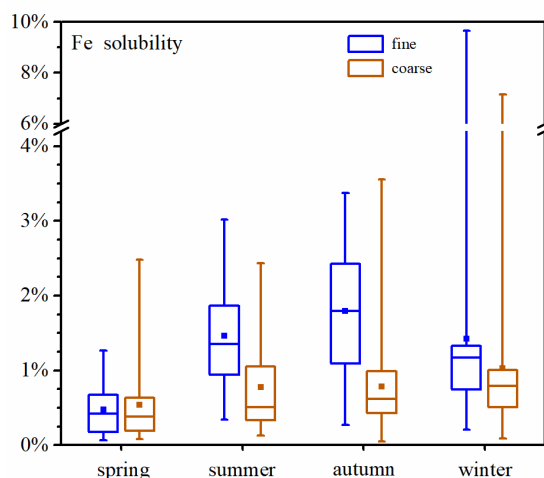
## 269 **4 Aerosol Fe solubility**

### 270 **4.1 Seasonal variation of Fe solubility**

271 Figure 4 and Table A1 display aerosol Fe solubility at Xi'an in different seasons. Fe  
272 solubility was in the range of 0.08-2.48%, 0.13-2.44%, 0.05-3.55% and 0.09-7.16% for coarse  
273 particles in spring, summer, autumn and winter, and the median values were 0.38%, 0.51%,  
274 0.62% and 0.79%; for fine particles, Fe solubility was in the range of 0.06-1.26%, 0.34-3.02%,



275 0.27-3.37% and 0.21-9.65% in spring, summer, autumn and winter, and the median values  
276 were 0.42%, 1.35%, 1.79% and 1.17%.



277

278 **Figure 4.** Seasonal variations of aerosol Fe solubility for fine and coarse particles at Xi'an.

279

280 No significant difference in Fe solubility was found between coarse and fine particles at  
281 Xi'an in spring (paired *t*-test,  $p=0.17$ ,  $\alpha=0.05$ ). In addition, the median values of Fe solubility  
282 were both  $<0.5\%$  for coarse and fine particles in spring, similar to desert dust (Schroth et al.,  
283 2009; Shi et al., 2011b; Oakes et al., 2012b; Li et al., 2022), and this was because Xi'an was  
284 frequently affected by desert dust aerosol in spring. In the other three seasons (summer, autumn  
285 and winter), Fe solubility was significantly higher in fine particles than coarse particles (paired  
286 *t*-test,  $p<0.01$ ,  $\alpha=0.05$ ); furthermore, in these three seasons the median Fe solubility was  $>1\%$   
287 for fine particles and  $>0.5\%$  for coarse particles. For coarse particles, Fe solubility was highest  
288 in winter and lowest in spring, while no significant difference was found between summer and  
289 autumn (*t*-test,  $p=0.95$ ,  $\alpha=0.05$ ); for fine particles, Fe solubility can be described by the



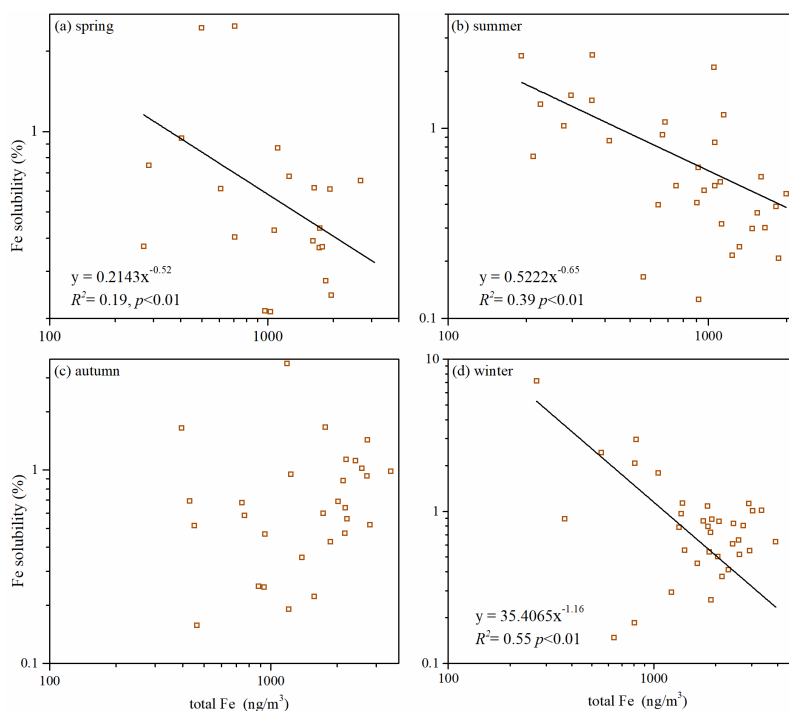


290 following order: autumn > summer > winter > spring.

291 A number of field measurements (Hsu et al., 2005; Baker and Jickells, 2006; Sedwick et  
292 al., 2007; Kumar et al., 2010; Sholkovitz et al., 2012; Winton et al., 2015; Shelley et al., 2018;  
293 Yang et al., 2022) found inverse dependence of Fe solubility on total Fe (and Al). As shown in  
294 Figures 5 and S8, Fe solubility was also observed in our work to decrease with total Fe for  
295 coarse and fine particles in three seasons (spring, summer and winter), and such dependence  
296 can be fitted using Eq. (1):

297 
$$f_s(Fe) = a \times [Fe]_T^{-b} \quad (1)$$

298 where  $f_s(Fe)$  is Fe solubility and  $[Fe]_T$  is total Fe concentration. As shown in Figures S9-S10,  
299 such inverse dependence was also observed between Fe solubility and total Al in these three  
300 seasons.



301

302 **Figure 5.** Fe solubility versus total Fe for coarse particles in different seasons: (a) spring; (b)

303 summer; (c) autumn; (d) winter.

304

305 However, no obvious relationship between Fe solubility and total Fe or total Al was found

306 in autumn. Such inverse dependence was not found in some previous studies either (Paris et

307 al., 2010; Oakes et al., 2012a), and was found for fine particles but not for coarse particles at

308 Qingdao in the winter by our previous work (Zhang et al., 2022). Therefore, one may conclude

309 that the inverse dependence of Fe solubility on total Fe (or Al), though frequently observed, is

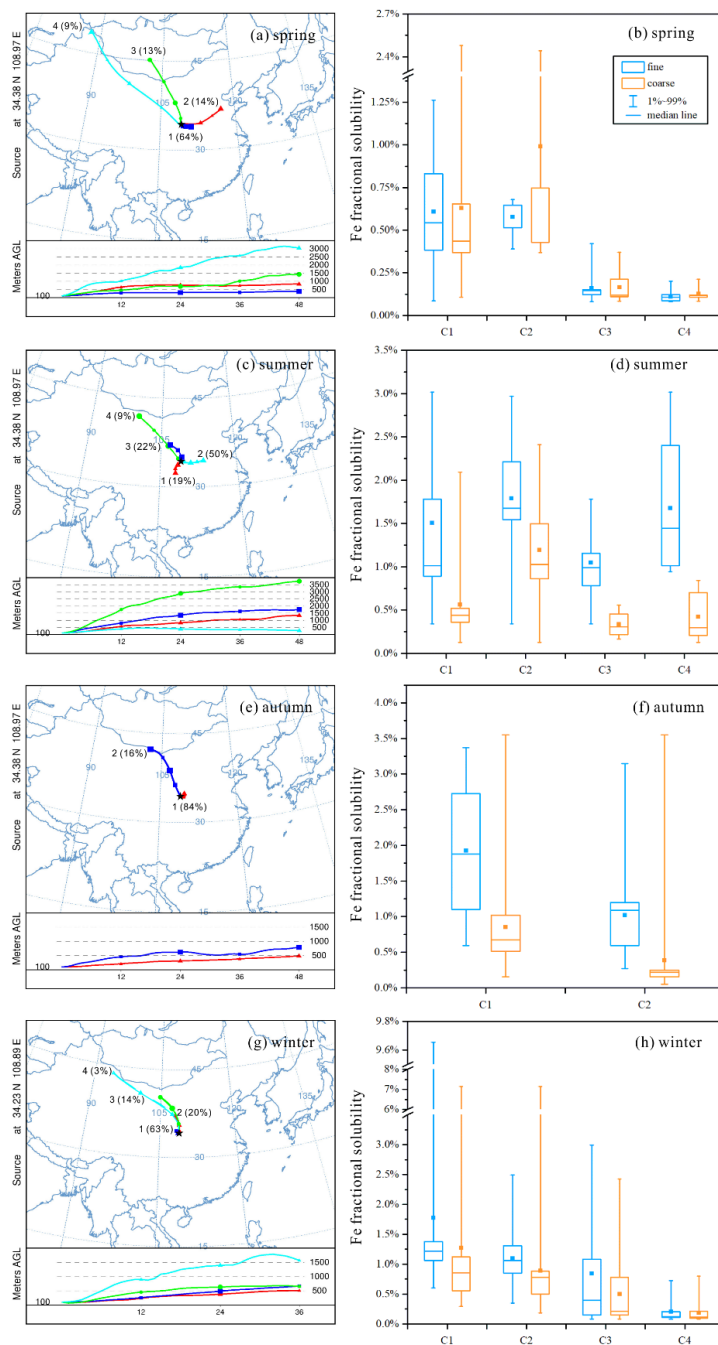
310 not a universe rule.

311 **4.2 Influence of air mass sources on Fe solubility**



312 Back trajectories obtained for our campaign were clustered, and we further examined the  
313 dependence of Fe solubility on air mass cluster types in different seasons. In spring (Figure 6a),  
314 air mass cluster C1 originated locally and C2 originated from North China Plain with severe  
315 air pollution, while C3 and C4 presented air mass arriving from desert regions in the north and  
316 northwest after long-distance transport (compared to C1 and C2); as shown in Figure 6b, Fe  
317 solubility in coarse and fine particles was significantly higher for C1 and C2, when compared  
318 to C3 and C4.

319 In autumn (Figure 6e), air mass cluster C1 originated locally and C2 was transported from  
320 desert regions in the north/northwest, and Fe solubility was much higher for C1 than C2 (Figure  
321 6f). In winter (Figure 6g), air mass cluster C1 originated locally while C2, C3 and C4 originated  
322 from desert regions in the north and northwest, and the transport distance increased from C2 to  
323 C4; as shown in Figure 6h, Fe solubility followed the order  $C1 > C2 > C3 > C4$ , decreasing  
324 with increase in transport distance. In contrast to other three seasons, no obvious dependence  
325 of Fe solubility on air mass clusters was found in summer (Figure 6d).





327 **Figure 6.** The mean backward trajectory clusters obtained by HYSPLIT for (a) spring, (c)  
328 summer, (e) autumn, and (g) winter; Fe solubility in fine and coarse particles from different air  
329 mass clusters in (b) spring, (d) summer, (f) autumn, and (h) winter. C1-C4 represent different  
330 air mass clusters.

331

332 To summarize, our work found that in spring, autumn and winter, Fe solubility at Xi'an  
333 was significantly higher when air masses originated from local and nearby regions, when  
334 compared to those arriving from desert regions after long-distance transport. The reason is that  
335 the contribution of anthropogenic emissions to aerosol Fe was elevated for air masses originating  
336 from local and nearby sources (when compared to air masses originating from desert regions),  
337 and anthropogenic aerosol Fe had higher solubility than desert dust (Schroth et al., 2009; Fu et  
338 al., 2012; Oakes et al., 2012b). Similar to our work, over the Sargasso Sea aerosol Fe solubility  
339 was much lower in Saharan air masses than North American air masses (Sedwick et al., 2007).

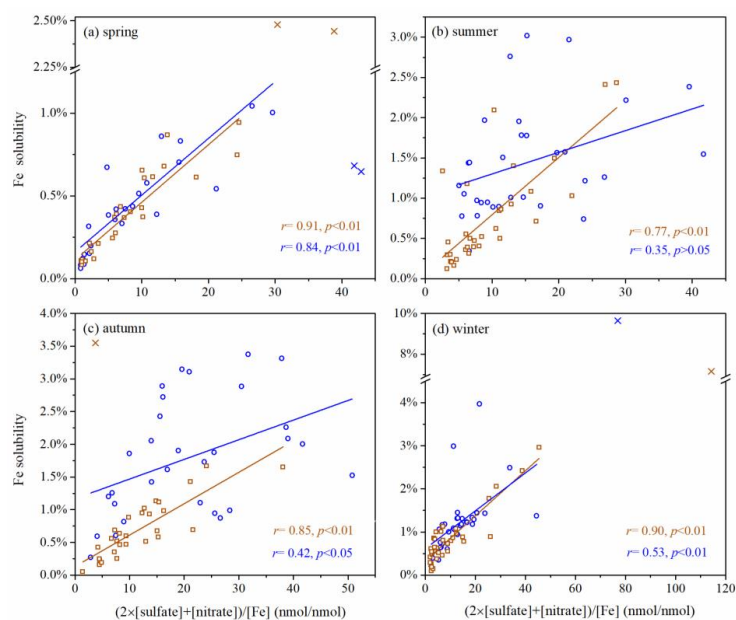
#### 340 **4.3 Effects of chemical aging**

341 Laboratory studies (Shi et al., 2011a; Chen and Grassian, 2013; Wang et al., 2018)  
342 suggested that chemical processing by acids, such as H<sub>2</sub>SO<sub>4</sub> and HNO<sub>3</sub>, could dissolve  
343 insoluble Fe and thus enhance aerosol Fe solubility. Some field studies found that aerosol Fe  
344 solubility was positively correlated with sulfate and/or nitrate (Shi et al., 2020; Zhu et al., 2020;  
345 Liu et al., 2021; Yang et al., 2022; Zhang et al., 2022), indicating enhancement of Fe solubility  
346 by atmospheric acid processing.

347 Figure 7 plots Fe solubility at Xi'an versus  $(2 \times [\text{sulfate}] + [\text{nitrate}]) / [\text{Fe}]$  (in nmol/nmol,



348 referred to as relative abundance of aerosol acidic species), the molar ratio of two major acidic  
349 species to total Fe in aerosol particles. For coarse particles, aerosol Fe solubility was well  
350 correlated with relative abundance of aerosol acidic species in all the four seasons ( $0.77 < r$   
351  $< 0.91$ ,  $p < 0.01$ ). For fine particles, good correlation was found in spring ( $r = 0.84$ ,  $p < 0.01$ ),  
352 moderate correlation was found in autumn and winter ( $0.42 < r < 0.53$ ,  $p < 0.01$ ), and no  
353 significant correlation was found in summer ( $r = 0.35$ ,  $p > 0.05$ ).



354  
355 **Figure 7.** Fe solubility versus  $(2 \times [\text{sulfate}] + [\text{nitrate}]) / [\text{Fe}]$  for fine and coarse particles in  
356 different seasons: (a) spring; (b) summer; (c) autumn; (d) winter.

357

358 Overall, correlations between Fe solubility and relative abundance of aerosol acidic  
359 species were always better for coarse particles than fine particles (Figure 7), indicating that  
360 acid processing may be more important in Fe solubility enhancement for coarse particles, when



361 compared to fine particles. A previous study (Zhang et al., 2022) also found that such  
362 correlation was better in coarse particles than fine particles in winter at Qingdao, a coastal city  
363 in northern China. Nevertheless, as discussed in Section 4.1, Fe solubility was higher in fine  
364 particles than coarse particles. This may imply that primary emission of non-desert-dust Fe  
365 (anthropogenic Fe) with higher solubility (Schroth et al., 2009; Oakes et al., 2012b) was more  
366 important for Fe solubility enhancement in fine particles than coarse particles.

367 It was suggested by laboratory studies (Chen and Grassian, 2013; Paris and Desboeufs,  
368 2013; Wang et al., 2017) that atmospheric organic ligands, such as oxalate, could increase  
369 aerosol Fe solubility via ligand-promoted dissolution. As shown in Figure S11, our present  
370 work found that good correlation between Fe solubility with [oxalate]/[Fe] (in nmol/nmol) was  
371 found for coarse particles ( $0.70 < r < 0.88$ ,  $p < 0.01$ ) and moderate correlation was found for fine  
372 particles ( $0.40 < r < 0.67$ ,  $p < 0.01$ ) at Xi'an. Positive correlation between Fe solubility and oxalate  
373 was also observed previously at Atlanta, USA (Yang and Weber, 2022), Toronto, Canada (Tao  
374 et al., 2022) and Qingdao, China (Zhang et al., 2022).

375 We note that good correlation between Fe solubility and aerosol oxalate does not  
376 necessarily mean Fe solubility enhancement by Fe-oxalate complexation. For example, it was  
377 suggested that Fe could promote the formation of oxalate in aerosol particles (Tao and Murphy,  
378 2019; Zhang et al., 2019), and thus good correlation between Fe solubility and oxalate could  
379 also imply enhanced formation of oxalate by dissolved Fe. In addition, similar to sulfate and  
380 nitrate, the major source of oxalate in the troposphere was secondary formation  
381 (Myriokefalitakis et al., 2011; Kawamura and Bikkina, 2016), and in this aspect good

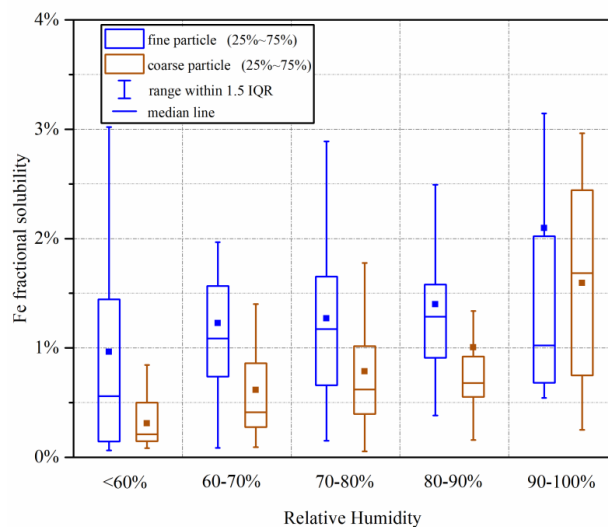


382 correlation between Fe solubility and relative abundance of oxalate could also indicate the  
383 importance of secondary formation of dissolved aerosol Fe.

### 384 **5 Discussion: roles of RH and aerosol acidity**

385 Figure 8 reveals the importance of RH in regulating aerosol Fe solubility. When RH was  
386 increased from <60% to 60-70%, significant increase in Fe solubility was observed for both  
387 coarse and fine particles. Sun et al. (2018) investigated hygroscopicity of aerosol particles  
388 collected in North China, and found that most particles examined started to become deliquesced  
389 when RH was increased to ~60%. The deliquescence RH reported for ambient aerosol particles  
390 (Sun et al., 2018) coincided roughly with the RH threshold at which large increase in aerosol  
391 Fe solubility was observed in our work. Previous studies (Shi et al., 2020; Zhu et al., 2020; Zhu  
392 et al., 2022) also highlighted that RH and thus aerosol liquid water could substantially affect  
393 Fe solubility. For examples, Zhu et al. (2020) measured Fe solubility at four cities in eastern  
394 China in December 2017, and found that Fe solubility at >50% RH was significantly larger  
395 than that at <50% RH.





396

397 **Figure 8.** Fe solubility in different relative humidity ranges for fine and coarse particles.

398 (RH<60%: 18 days; 60%<RH<70%: 23 days; 70%<RH<80%: 48 days; 80%<RH<90%: 28

399 days; RH>90%: 10 days).

400

401 In addition, as shown in Figure 8, when RH was increased from 80-90% to >90%, median

402 Fe solubility was remarkably increased from 0.67% to 1.68% for coarse particles. Similar to

403 our work, Shi et al. (2020) also found that aerosol Fe solubility at Qingdao was significantly

404 increased under foggy weather when compared to other weather conditions. Both Shi et al.

405 (2020) and we suggested that high RH could promote Fe dissolution via acid processing.

406 We further examined the impact of aerosol acidity on Fe solubility, and the results are

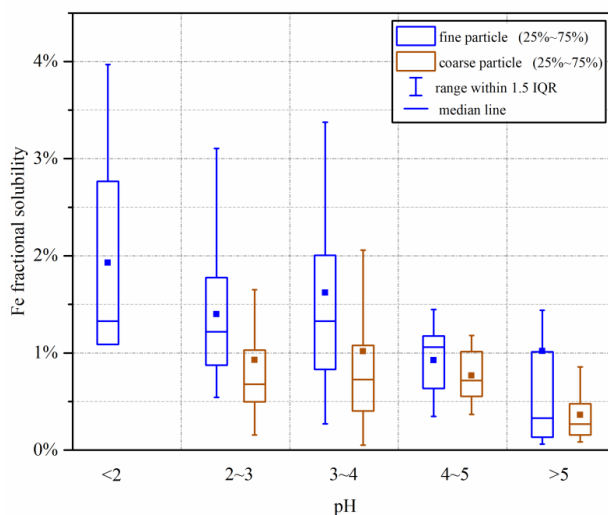
407 displayed in Figure 9. For coarse particles, increase in pH did not lead to apparent change in

408 Fe solubility as long as aerosol pH was <5; however, Fe solubility was greatly decreased when

409 aerosol pH was increased to >5. For fine particles, Fe solubility continuously decreased with



410 increasing aerosol pH (from  $<2$  to  $>5$ ). Previous work carried out at six Canadian sites (Tao  
411 and Murphy, 2019) and Atlanta (Georgia, USA) (Wong et al., 2020; Yang and Weber, 2022)  
412 also reported higher Fe solubility at lower aerosol pH. Similar to our previous work at Qingdao  
413 in the winter (Zhang et al., 2022), our current study found that for coarse and fine particles at  
414 Xi'an, aerosol pH was mostly  $<4$  when Fe solubility exceeded 1% (Figure S12). It should be  
415 pointed out that for some samples collected at Xi'an, Fe solubility could still be very low ( $<1\%$ )  
416 even when aerosol pH was low and RH was high (Figure S12). In addition, as shown in Figure 9,  
417 at a given pH range Fe solubility was always higher in fine particles than coarse particles; this  
418 may again imply that anthropogenic and pyrogenic Fe played a more important role in Fe  
419 solubility enhancement in fine particles at Xi'an, when compared to coarse particles.



420  
421 **Figure 9.** Fe solubility in different pH ranges for fine and coarse particles at Xi'an.  
422



423 At Xi'an, Fe solubility was higher in summer (median: 1.35%) and autumn (median: 1.79)  
424 than spring (median: 0.42) and winter (1.17%) for fine particles, and was also higher in summer  
425 (median: 0.51%) and autumn (0.62%) than spring (median: 0.79%). Meanwhile, our work  
426 found that aerosol pH values for both coarse and fine particles were lower ( $t$ -test,  $p < 0.01$ ,  
427  $\alpha = 0.05$ ) in summer and autumn than spring and winter (Table S5 and Figure S13). As a result,  
428 lower aerosol pH (thus higher aerosol acidity) in summer and autumn may at least partly  
429 explain the observed higher Fe solubility in these two seasons. Our results were corroborated  
430 by a previous study (Yang and Weber, 2022) which found that compared to the cold season,  
431 higher Fe solubility was found at Atlanta (Georgia, USA) in the warm season when aerosol pH  
432 was lower.

## 433 **6 Summary and conclusion**

434 Our work investigated total Fe, dissolved Fe and Fe solubility for coarse ( $> 1 \mu\text{m}$ ) and fine  
435 ( $< 1 \mu\text{m}$ ) particles in four different seasons at Xi'an, a megacity in northwestern China impacted  
436 by anthropogenic emissions and desert dust. Total Fe concentrations in coarse particles were  
437 lowest in summer and similar in the other three seasons, while for fine particles total Fe  
438 concentrations were also lowest in summer and highest in spring. Good correlations were found  
439 between total Fe and total Al for both coarse and fine particles in all the four seasons,  
440 suggesting desert dust aerosol as the major source of total Fe regardless of particle size (below  
441 or above  $1 \mu\text{m}$ ) and season.

442 Dissolved Fe concentrations were higher in autumn and winter than spring and summer  
443 for coarse particles; for fine particles, dissolved Fe concentrations were highest in winter,



444 followed by autumn, and lowest in spring and summer. Compared to other seasons, although  
445 total Fe concentrations were evaluated in spring due to the impacts of desert dust, increase in  
446 dissolved Fe levels was not observed. This may imply that the occurrence of desert dust aerosol  
447 may not necessarily lead to increase in dissolved Fe concentrations, as also revealed in our  
448 previous study (Zhang et al., 2022) carried out at a coastal city in northern China. Dissolved  
449 Fe was significantly lower for coarse particles (compared to fine particles) in all the four  
450 seasons, although total Fe in coarse particles were higher than or similar to fine particles in  
451 three seasons (but not spring), implying higher Fe solubility in fine particles. Overall the  
452 correlation between dissolved Fe and total Al was rather weak, suggesting that desert dust may  
453 not contribute dominantly to dissolved Fe at Xi'an, although it was always the major source of  
454 total Fe.

455 Highest Fe solubility was observed in winter for coarse particles and in autumn for fine  
456 particles; meanwhile, lowest Fe solubility was observed in spring for both coarse and fine  
457 particles, with median Fe solubility both below 0.5%. Compared to coarse particles, Fe  
458 solubility was similar for fine particles in spring but significantly higher in the other three  
459 seasons. Inverse dependence of Fe solubility on total Fe concentration, was observed for coarse  
460 and fine particles in spring, summer and winter, while there was no such dependence for either  
461 fine or coarse particles in autumn. Furthermore, aerosol Fe solubility was higher in air masses  
462 originating from local and nearby regions than those arriving from desert regions after long-  
463 distance transport in three seasons (spring, autumn and winter), while no apparent dependence  
464 of Fe solubility on air mass origins was found in summer.



465           Our work found better correlation between Fe solubility and relative abundance of aerosol  
466   acidic species for coarse particles than fine particles in all the four seasons, probably suggesting  
467   that acid processing was more important for Fe solubility enhancement in coarse particles. This  
468   may further mean that non-desert-dust Fe (e.g., anthropogenic and biomass burning Fe) was  
469   more important for Fe solubility enhancement in fine particles, since Fe solubility was higher  
470   in fine particles than coarse particles. We also found that overall Fe solubility increased with  
471   RH and acid acidity for coarse and fine particles, underscoring the importance of aerosol liquid  
472   water and aerosol acidity in enhancing Fe solubility via acid processing. Our work further  
473   found that at a given pH range aerosol Fe solubility was always higher in fine particles than  
474   coarse particles.

475

476



477 **Appendices**

478 **Table A1.** Overview of total Fe (in ng/m<sup>3</sup>), dissolved Fe (in ng/m<sup>3</sup>) and Fe solubility (in %) for  
479 fine and coarse particles in different seasons at Xi'an.

fine particles				coarse particles		
<b>Spring</b>	<b>range</b>	<b>median</b>	<b>average</b>	<b>range</b>	<b>median</b>	<b>average</b>
total Fe	206-12144	2925	3717±3387	270-3095	1626	1504±800
dissolved Fe	1.1-21.4	9.2	10.0±5.5	1.0-17.5	4.2	5.9±4.5
Fe solubility	0.06-1.26	0.42	0.48±0.32	0.08-2.48	0.38	0.54±0.59
<b>Summer</b>	<b>range</b>	<b>median</b>	<b>average</b>	<b>range</b>	<b>median</b>	<b>average</b>
total Fe	164-1591	719	721±366	191-1992	942	950±524
dissolved Fe	2.6-22.9	8.5	9.7±5.6	0.9-22.0	4.6	5.6±4.0
Fe solubility	0.34-3.02	1.35	1.46±0.67	0.13-2.44	0.51	0.78±0.63
<b>Autumn</b>	<b>range</b>	<b>median</b>	<b>average</b>	<b>range</b>	<b>median</b>	<b>average</b>
total Fe	196-2631	934	958±516	395-3492	1651	1638±830
dissolved Fe	2.1-33.7	15.4	16.5±10.1	0.7-42.2	10.3	13.5±12.2
Fe solubility	0.27-3.37	1.79	1.80±0.88	0.05-3.55	0.62	0.79±0.67
<b>Winter</b>	<b>range</b>	<b>median</b>	<b>average</b>	<b>range</b>	<b>median</b>	<b>average</b>
total Fe	257-4268	1942	2058±1037	269-3924	1850	1831±866
dissolved Fe	5.0-89.5	17.4	22.7±16.8	0.9-33.8	14.7	14.5±8.3
Fe solubility	0.21-9.65	1.17	1.43±1.58	0.09-7.16	0.79	1.03±1.22

480

481 **Data availability.**

482 Data are available upon request (Mingjin Tang: mingjintang@gig.ac.cn).

483 **Competing interests.**

484 The authors declare that they have no conflict of interest.

485 **Author contribution.**



486 **Huanhuan Zhang:** investigation, formal analysis, writing-original draft, writing-review &  
487 editing; **Rui Li:** investigation, writing-original draft; **Chengpeng Huang:** investigation;  
488 **Xiaofei Li:** investigation; **Shuwei Dong:** investigation; **Fu Wang:** investigation; **Tingting Li:**  
489 investigation; **Yizhu Chen:** investigation; **Guohua Zhang:** resource, writing-review & editing;  
490 **Yan Ren:** resource; **Qingcai Chen:** resource; **Ru-jin Huang:** resource; **Siyu Chen:** writing-  
491 review & editing; **Xinming Wang:** resource; **Mingjin Tang:** conceptualization, formal  
492 analysis, writing-original draft, writing-review & editing.

493 **Financial support.**

494 This work was sponsored by National Natural Science Foundation of China (42022050 and  
495 42277088), China Postdoctoral Science Foundation (2021M703222), Guangdong Foundation  
496 for Program of Science and Technology Research (2019B121205006 and 2020B1212060053),  
497 Guangdong Province (2017GC010501) and the CAS Pioneer Hundred Talents program.

498 **Acknowledgement.**

499 We would like to thank Dr. Shiguo Jia at Sun Yat-sen University for assistance in air mass  
500 back trajectory analysis.

501

502



503 **References**

- 504 Abbaspour, N., Hurrell, R., and Kelishadi, R.: Review on iron and its importance for  
505 human health, *J. Res. Med. Sci.*, 19, 164-174, 2014.
- 506 Alexander, B., Park, R. J., Jacob, D. J., and Gong, S. L.: Transition metal-catalyzed  
507 oxidation of atmospheric sulfur: Global implications for the sulfur budget, *J. Geophys. Res.-*  
508 *Atmos.*, 114, D02309, doi: 02310.01029/02008jd010486, 2009.
- 509 Baker, A. R. and Jickells, T. D.: Mineral particle size as a control on aerosol iron solubility,  
510 *Geophys. Res. Lett.*, 33, L17608, doi: 17610.11029/12006GL026557, 2006.
- 511 Baker, A. R., Kanakidou, M., Nenes, A., Myriokefalitakis, S., Croot, P. L., Duce, R. A.,  
512 Gao, Y., Guieu, C., Ito, A., Jickells, T. D., Mahowald, N. M., Middag, R., Perron, M. M. G.,  
513 Sarin, M. M., Shelley, R., and Turner, D. R.: Changing atmospheric acidity as a modulator of  
514 nutrient deposition and ocean biogeochemistry, *Science Advances*, 7, eabd8800,  
515 10.1126/sciadv.abd8800, 2021.
- 516 Baker, J.: A cluster analysis of long range air transport pathways and associated pollutant  
517 concentrations within the UK, *Atmos. Environ.*, 44, 563-571, 2010.
- 518 Boyd, P. W. and Ellwood, M. J.: The biogeochemical cycle of iron in the ocean, *Nature*  
519 *Geosci.*, 3, 675-682, 2010.
- 520 Cao, J. J. and Cui, L.: Current Status, Characteristics and Causes of Particulate Air  
521 Pollution in the Fenwei Plain, China: A Review, *J. Geophys. Res.-Atmos.*, 126,  
522 e2020JD034472, doi: 034410.031029/032020JD034472, 2021.
- 523 Cao, J. J., Wang, Q. Y., Chow, J. C., Watson, J. G., Tie, X. X., Shen, Z. X., Wang, P., and  
524 An, Z. S.: Impacts of aerosol compositions on visibility impairment in Xi'an, China, *Atmos.*  
525 *Environ.*, 59, 559-566, 2012.
- 526 Chen, H. H. and Grassian, V. H.: Iron Dissolution of Dust Source Materials during  
527 Simulated Acidic Processing: The Effect of Sulfuric, Acetic, and Oxalic Acids, *Environ. Sci.*  
528 *Tech.*, 47, 10312-10321, 2013.
- 529 Chen, Q. C., Hua, X. Y., Li, J. W., Chang, T., and Wang, Y. Q.: Diurnal evolutions and  
530 sources of water-soluble chromophoric aerosols over Xi'an during haze event, in Northwest  
531 China, *Sci. Total Environ.*, 786, 147412, 10.1016/j.scitotenv.2021.147412, 2021.
- 532 Chen, Y. and Siefert, R. L.: Seasonal and spatial distributions and dry deposition fluxes  
533 of atmospheric total and labile iron over the tropical and subtropical North Atlantic Ocean, *J.*  
534 *Geophys. Res.-Atmos.*, 109, D09305, doi: 09310.01029/02003JD003958, 2004.
- 535 Draxier, R. R. and Hess, G. D.: An overview of the HYSPLIT\_4 modelling system for  
536 trajectories, dispersion and deposition, *Aust. Meteorol. Mag.*, 47, 295-308, 1998.
- 537 Fang, T., Guo, H. Y., Zeng, L. H., Verma, V., Nenes, A., and Weber, R. J.: Highly Acidic  
538 Ambient Particles, Soluble Metals, and Oxidative Potential: A Link between Sulfate and  
539 Aerosol Toxicity, *Environ. Sci. Technol.*, 51, 2611-2620, 2017.
- 540 Fountoukis, C. and Nenes, A.: ISORROPIA II: a computationally efficient  
541 thermodynamic equilibrium model for  $K^+$ - $Ca^{2+}$ - $Mg^{2+}$ - $NH_4^+$ - $Na^+$ - $SO_4^{2-}$ - $NO_3^-$ - $Cl^-$ - $H_2O$  aerosols,  
542 *Atmos. Chem. Phys.*, 7, 4639-4659, 2007.





- 543 Fu, H. B., Lin, J., Shang, G. F., Dong, W. B., Grassian, V. H., Carmichael, G. R., Li, Y.,  
544 and Chen, J. M.: Solubility of Iron from Combustion Source Particles in Acidic Media Linked  
545 to Iron Speciation, *Environ. Sci. Technol.*, 46, 11119-11127, 2012.
- 546 Guo, H., Xu, L., Bougiatioti, A., Cerully, K. M., Capps, S. L., Hite Jr, J. R., Carlton, A.  
547 G., Lee, S. H., Bergin, M. H., Ng, N. L., Nenes, A., and Weber, R. J.: Fine-particle water and  
548 pH in the southeastern United States, *Atmos. Chem. Phys.*, 15, 5211-5228, 2015.
- 549 Hamilton, D. S., Scanza, R. A., Rathod, S. D., Bond, T. C., Kok, J. F., Li, L., Matsui, H.,  
550 and Mahowald, N. M.: Recent (1980 to 2015) Trends and Variability in Daily-to-Interannual  
551 Soluble Iron Deposition from Dust, Fire, and Anthropogenic Sources, *Geophys. Res. Lett.*, 47,  
552 e2020GL089688, 2020.
- 553 Hennigan, C. J., Izumi, J., Sullivan, A. P., Weber, R. J., and Nenes, A.: A critical  
554 evaluation of proxy methods used to estimate the acidity of atmospheric particles, *Atmos.*  
555 *Chem. Phys.*, 15, 2775-2790, 2015.
- 556 Hsu, S.-C., Lin, F.-J., and Jeng, W.-L.: Seawater solubility of natural and anthropogenic  
557 metals within ambient aerosols collected from Taiwan coastal sites, *Atmos. Environ.*, 39, 3989-  
558 4001, 2005.
- 559 Huang, X., Song, Y., Zhao, C., Li, M., Zhu, T., Zhang, Q., and Zhang, X.: Pathways of  
560 sulfate enhancement by natural and anthropogenic mineral aerosols in China, *J. Geophys. Res.-*  
561 *Atmos.*, 119, 14165-14179, 2014.
- 562 Ito, A., Ye, Y., Baldo, C., and Shi, Z. B.: Ocean fertilization by pyrogenic aerosol iron,  
563 *NPJ Clim. Atmos. Sci.*, 4, 30, doi: 10.1038/s41612-41021-00185-41618, 2021.
- 564 Ito, A., Myriokefalitakis, S., Kanakidou, M., Mahowald, N. M., Scanza, R. A., Hamilton,  
565 D. S., Baker, A. R., Jickells, T., Sarin, M., Bikkina, S., Gao, Y., Shelley, R. U., Buck, C. S.,  
566 Landing, W. M., Bowie, A. R., Perron, M. M. G., Guieu, C., Meskhidze, N., Johnson, M. S.,  
567 Feng, Y., Kok, J. F., Nenes, A., and Duce, R. A.: Pyrogenic iron: The missing link to high iron  
568 solubility in aerosols, *Science Adv.*, 5, eaau7671, doi: 7610.1126/sciadv.aau7671, 2019.
- 569 Jickells, T. D., An, Z. S., Andersen, K. K., Baker, A. R., Bergametti, G., Brooks, N., Cao,  
570 J. J., Boyd, P. W., Duce, R. A., Hunter, K. A., Kawahata, H., Kubilay, N., laRoche, J., Liss, P.  
571 S., Mahowald, N., Prospero, J. M., Ridgwell, A. J., Tegen, I., and Torres, R.: Global Iron  
572 Connections between Desert Dust, Ocean Biogeochemistry, and Climate, *Science*, 308, 67-71,  
573 2005.
- 574 Kawamura, K. and Bikkina, S.: A review of dicarboxylic acids and related compounds in  
575 atmospheric aerosols: Molecular distributions, sources and transformation, *Atmos. Res.*, 170,  
576 140-160, 2016.
- 577 Kelly, F. J.: Oxidative stress: Its role in air pollution and adverse health effects,  
578 *Occupational and Environmental Medicine*, 60, 612-616, 2003.
- 579 Kumar, A., Sarin, M. M., and Srinivas, B.: Aerosol iron solubility over Bay of Bengal:  
580 Role of anthropogenic sources and chemical processing, *Mar. Chem.*, 121, 167-175, 2010.
- 581 Li, R., Zhang, H. H., Wang, F., He, Y. T., Huang, C. P., Luo, L., Dong, S. W., Jia, X. H.,  
582 and Tang, M. J.: Mass fractions, solubility, speciation and isotopic compositions of iron in coal  
583 and municipal waste fly ash, *Sci. Total Environ.*, 838, 155974, 2022.



- 584 Li, W. J., Xu, L., Liu, X. H., Zhang, J. C., Lin, Y. T., Yao, X. H., Gao, H. W., Zhang, D.  
585 Z., Chen, J. M., Wang, W. X., Harrison, R. M., Zhang, X. Y., Shao, L. Y., Fu, P. Q., Nenes,  
586 A., and Shi, Z. B.: Air pollution–aerosol interactions produce more bioavailable iron for ocean  
587 ecosystems, *Science Adv.*, 3, e1601749, 2017.
- 588 Liu, L., Lin, Q., Liang, Z., Du, R., Zhang, G., Zhu, Y., Qi, B., Zhou, S., and Li, W.:  
589 Variations in concentration and solubility of iron in atmospheric fine particles during the  
590 COVID-19 pandemic: An example from China, *Gondwana Research*, 97, 138-144, 2021.
- 591 Liu, M. X., Matsui, H., Hamilton, D. S., Lamb, K. D., Rathod, S. D., Schwarz, J. P., and  
592 Mahowald, N. M.: The underappreciated role of anthropogenic sources in atmospheric soluble  
593 iron flux to the Southern Ocean, *Npj Climate and Atmospheric Science*, 5, 28, 10.1038/s41612-  
594 022-00250-w, 2022.
- 595 Mahowald, N. M., Hamilton, D. S., Mackey, K. R. M., Moore, J. K., Baker, A. R., Scanza,  
596 R. A., and Zhang, Y.: Aerosol trace metal leaching and impacts on marine microorganisms,  
597 *Nature Comm.*, 9, 2614, 2018.
- 598 Martin, J. H.: Glacial-interglacial CO<sub>2</sub> change: the iron hypothesis, *Paleoceanography*, 5,  
599 1-13, 1990.
- 600 Martin, L. R. and Good, T. W.: Catalyzed oxidation of sulfur dioxide in solution: The  
601 iron-manganese synergism, *Atmos. Environ.*, 25A, 2395-2399, 1991.
- 602 Meskhidze, N., Volker, C., Al-Abadleh, H. A., Barbeau, K., Bressac, M., Buck, C., Bundy,  
603 R. M., Croot, P., Feng, Y., Ito, A., Johansen, A. M., Landing, W. M., Mao, J. Q.,  
604 Myriokefalitakis, S., Ohnemus, D., Pasquier, B., and Ye, Y.: Perspective on identifying and  
605 characterizing the processes controlling iron speciation and residence time at the atmosphere-  
606 ocean interface, *Mar. Chem.*, 217, 103704, 2019.
- 607 Moore, C. M., Mills, M. M., Achterberg, E. P., Geider, R. J., LaRoche, J., Lucas, M. I.,  
608 McDonagh, E. L., Pan, X., Poulton, A. J., Rijkenberg, M. J. A., Suggett, D. J., Ussher, S. J.,  
609 and Woodward, E. M. S.: Large-scale distribution of Atlantic nitrogen fixation controlled by  
610 iron availability, *Nature Geosci.*, 2, 867-871, 2009.
- 611 Myriokefalitakis, S., Tsigaridis, K., Mihalopoulos, N., Sciare, J., Nenes, A., Kawamura,  
612 K., Segers, A., and Kanakidou, M.: In-cloud oxalate formation in the global troposphere: a 3-  
613 D modeling study, *Atmos. Chem. Phys.*, 11, 5761-5782, 2011.
- 614 Myriokefalitakis, S., Ito, A., Kanakidou, M., Nenes, A., Krol, M. C., Mahowald, N. M.,  
615 Scanza, R. A., Hamilton, D. S., Johnson, M. S., Meskhidze, N., Kok, J. F., Guieu, C., Baker,  
616 A. R., Jickells, T. D., Sarin, M. M., Bikkina, S., Shelley, R., Bowie, A., Perron, M. M. G., and  
617 Duce, R. A.: Reviews and syntheses: the GESAMP atmospheric iron deposition model  
618 intercomparison study, *Biogeosciences*, 15, 6659-6684, 2018.
- 619 Oakes, M., Weber, R. J., Lai, B., Russell, A., and Ingall, E. D.: Characterization of iron  
620 speciation in urban and rural single particles using XANES spectroscopy and micro X-ray  
621 fluorescence measurements: investigating the relationship between speciation and fractional  
622 iron solubility, *Atmos. Chem. Phys.*, 12, 745-756, 2012a.



- 623 Oakes, M., Ingall, E. D., Lai, B., Shafer, M. M., Hays, M. D., Liu, Z. G., Russell, A. G.,  
624 and Weber, R. J.: Iron Solubility Related to Particle Sulfur Content in Source Emission and  
625 Ambient Fine Particles, *Environ. Sci. Technol.*, 46, 6637-6644, 2012b.
- 626 Paris, R. and Desboeufs, K. V.: Effect of atmospheric organic complexation on iron-  
627 bearing dust solubility, *Atmos. Chem. Phys.*, 13, 4895-4905, 2013.
- 628 Paris, R., Desboeufs, K. V., and Journet, E.: Variability of dust iron solubility in  
629 atmospheric waters: Investigation of the role of oxalate organic complexation, *Atmos. Environ.*,  
630 45, 6510-6517, 2011.
- 631 Paris, R., Desboeufs, K. V., Formenti, P., Nava, S., and Chou, C.: Chemical  
632 characterisation of iron in dust and biomass burning aerosols during AMMA-SOP0/DABEX:  
633 implication for iron solubility, *Atmos. Chem. Phys.*, 10, 4273-4282, 2010.
- 634 Pye, H. O. T., Nenes, A., Alexander, B., Ault, A. P., Barth, M. C., Clegg, S. L., Collett Jr,  
635 J. L., Fahey, K. M., Hennigan, C. J., Herrmann, H., Kanakidou, M., Kelly, J. T., Ku, I. T.,  
636 McNeill, V. F., Riemer, N., Schaefer, T., Shi, G., Tilgner, A., Walker, J. T., Wang, T., Weber,  
637 R., Xing, J., Zaveri, R. A., and Zuend, A.: The acidity of atmospheric particles and clouds,  
638 *Atmos. Chem. Phys.*, 20, 4809-4888, 2020.
- 639 Sakata, K., Kurisu, M., Takeichi, Y., Sakaguchi, A., Tanimoto, H., Tamenori, Y., Matsuki,  
640 A., and Takahashi, Y.: Iron (Fe) speciation in size-fractionated aerosol particles in the Pacific  
641 Ocean: The role of organic complexation of Fe with humic-like substances in controlling Fe  
642 solubility, *Atmos. Chem. Phys.*, 22, 9461-9482, 2022.
- 643 Schroth, A. W., Crusius, J., Sholkovitz, E. R., and Bostick, B. C.: Iron solubility driven  
644 by speciation in dust sources to the ocean, *Nature Geosci.*, 2, 337-340, 2009.
- 645 Sedwick, P. N., Sholkovitz, E. R., and Church, T. M.: Impact of anthropogenic  
646 combustion emissions on the fractional solubility of aerosol iron: Evidence from the Sargasso  
647 Sea, *Geochem. Geophys. Geosyst.*, Q10Q06, DOI: 10.1029/2007GC001586, 2007.
- 648 Seinfeld, J. H. and Pandis, S. N.: *Atmospheric Chemistry and Physics: From Air Pollution  
649 to Climate Change* (Third edition), Wiley Interscience, New York 2016.
- 650 Shelley, R. U., Landing, W. M., Ussher, S. J., Planquette, H., and Sarthou, G.: Regional  
651 trends in the fractional solubility of Fe and other metals from North Atlantic aerosols  
652 (GEOTRACES cruises GA01 and GA03) following a two-stage leach, *Biogeosciences*, 15,  
653 2271-2288, 2018.
- 654 Shi, J. H., Guan, Y., Ito, A., Gao, H. W., Yao, X. H., Baker, A. R., and Zhang, D. Z.: High  
655 Production of Soluble Iron Promoted by Aerosol Acidification in Fog, *Geophys. Res. Lett.*, 47,  
656 e2019GL086124, 10.1029/2019gl086124, 2020.
- 657 Shi, Z., Bonneville, S., Krom, M. D., Carslaw, K. S., Jickells, T. D., Baker, A. R., and  
658 Benning, L. G.: Iron dissolution kinetics of mineral dust at low pH during simulated  
659 atmospheric processing, *Atmos. Chem. Phys.*, 11, 995-1007, 2011a.
- 660 Shi, Z. B., Krom, M. D., Jickells, T. D., Bonneville, S., Carslaw, K. S., Mihalopoulos, N.,  
661 Baker, A. R., and Benning, L. G.: Impacts on iron solubility in the mineral dust by processes  
662 in the source region and the atmosphere: A review, *Aeolian Res.*, 5, 21-42, 2012.



- 663 Shi, Z. B., Woodhouse, M. T., Carslaw, K. S., Krom, M. D., Mann, G. W., Baker, A. R.,  
664 Savov, I., Fones, G. R., Brooks, B., Drake, N., Jickells, T. D., and Benning, L. G.: Minor effect  
665 of physical size sorting on iron solubility of transported mineral dust, *Atmos. Chem. Phys.*, 11,  
666 8459-8469, 2011b.
- 667 Sholkovitz, E. R., Sedwick, P. N., and Church, T. M.: Influence of anthropogenic  
668 combustion emissions on the deposition of soluble aerosol iron to the ocean: Empirical  
669 estimates for island sites in the North Atlantic, *Geochim. Cosmochim. Acta*, 73, 3981-4003,  
670 2009.
- 671 Sholkovitz, E. R., Sedwick, P. N., Church, T. M., Baker, A. R., and Powell, C. F.:  
672 Fractional solubility of aerosol iron: Synthesis of a global-scale data set, *Geochim. Cosmochim.*  
673 *Acta*, 89, 173-189, 2012.
- 674 Sun, J. X., Liu, L., Xu, L., Wang, Y. Y., Wu, Z. J., Hu, M., Shi, Z. B., Li, Y. J., Zhang, X.  
675 Y., Chen, J. M., and Li, W. J.: Key Role of Nitrate in Phase Transitions of Urban Particles:  
676 Implications of Important Reactive Surfaces for Secondary Aerosol Formation, *J. Geophys.*  
677 *Res.-Atmos.*, 123, 1234-1243, 2018.
- 678 Tagliabue, A., Bowie, A. R., Boyd, P. W., Buck, K. N., Johnson, K. S., and Saito, M. A.:  
679 The integral role of iron in ocean biogeochemistry, *Nature*, 543, 51-59, 2017.
- 680 Tang, W., Llorc, J., Weis, J., Perron, M. M. G., Basart, S., Li, Z., Sathyendranath, S.,  
681 Jackson, T., Sanz Rodriguez, E., Proemse, B. C., Bowie, A. R., Schallenberg, C., Strutton, P.  
682 G., Matear, R., and Cassar, N.: Widespread phytoplankton blooms triggered by 2019–2020  
683 Australian wildfires, *Nature*, 597, 370-375, 2021.
- 684 Tao, Y. and Murphy, J. G.: The Mechanisms Responsible for the Interactions among  
685 Oxalate, pH, and Fe Dissolution in PM<sub>2.5</sub>, *ACS Earth and Space Chem.*, 3, 2259-2265, 2019.
- 686 Tao, Y., Moravek, A., Furlani, T. C., Power, C. E., VandenBoer, T. C., Chang, R. Y. W.,  
687 Wiacek, A., and Young, C. J.: Acidity of Size-Resolved Sea-Salt Aerosol in a Coastal Urban  
688 Area: Comparison of Existing and New Approaches, *ACS Earth and Space Chemistry*, 6, 1239-  
689 1249, 2022.
- 690 Wang, Y., Salana, S., Yu, H., Puthussery, J. V., and Verma, V.: On the Relative  
691 Contribution of Iron and Organic Compounds, and Their Interaction in Cellular Oxidative  
692 Potential of Ambient PM<sub>2.5</sub>, *Environmental Science & Technology Letters*, 9, 680-686, 2022.
- 693 Wang, Y. Q., Wang, M. M., Li, S. P., Sun, H. Y., Mu, Z., Zhang, L. X., Li, Y. G., and  
694 Chen, Q. C.: Study on the oxidation potential of the water-soluble components of ambient  
695 PM<sub>2.5</sub> over Xi'an, China: Pollution levels, source apportionment and transport pathways,  
696 *Environ. Int.*, 136, 105515, 10.1016/j.envint.2020.105515, 2020.
- 697 Wang, Z., Fu, H., Zhang, L., Song, W., and Chen, J.: Ligand-Promoted Photoreductive  
698 Dissolution of Goethite by Atmospheric Low-Molecular Dicarboxylates, *J. Phys. Chem. A*,  
699 121, 1647-1656, 2017.
- 700 Wang, Z., Li, R., Cui, L., Fu, H., Lin, J., and Chen, J.: Characterization and acid-  
701 mobilization study for typical iron-bearing clay mineral, *J. Environ. Sci.*, 71, 222-232, 2018.



- 702 Winton, V. H. L., Bowie, A. R., Edwards, R., Keywood, M., Townsend, A. T., van der  
703 Merwe, P., and Bollhofer, A.: Fractional iron solubility of atmospheric iron inputs to the  
704 Southern Ocean, *Marine Chemistry*, 177, 20-32, 2015.
- 705 Wong, J. P. S., Yang, Y., Fang, T., Mulholland, J. A., Russell, A. G., Ebel, S., Nenes, A.,  
706 and Weber, R. J.: Fine Particle Iron in Soils and Road Dust Is Modulated by Coal-Fired Power  
707 Plant Sulfur, *Environ. Sci. Technol.*, 54, 7088-7096, 2020.
- 708 Yang, J., Ma, L., He, X., Au, W. C., Miao, Y., Wang, W. X., and Nah, T.: Measurement  
709 Report: Abundance and fractional solubilities of aerosol metals in urban Hong Kong: Insights  
710 into factors that control aerosol metal dissolution in an urban site in South China, *Atmos. Chem.*  
711 *Phys. Discuss.*, 2022, 1-31, 10.5194/acp-2022-597, 2022.
- 712 Yang, T., Chen, Y., Zhou, S., Li, H., Wang, F., and Zhu, Y.: Solubilities and deposition  
713 fluxes of atmospheric Fe and Cu over the Northwest Pacific and its marginal seas, *Atmos.*  
714 *Environ.*, 239, 117763, 2020.
- 715 Yang, Y. and Weber, R. J.: Ultrafiltration to characterize PM2.5 water-soluble iron and  
716 its sources in an urban environment, *Atmos. Environ.*, 286, 119246, 2022.
- 717 Zhang, G. H., Lin, Q. H., Peng, L., Yang, Y. X., Jiang, F., Liu, F. X., Song, W., Chen, D.  
718 H., Cai, Z., Bi, X. H., Miller, M., Tang, M. J., Huang, W. L., Wang, X. M., Peng, P. A., and  
719 Sheng, G. Y.: Oxalate Formation Enhanced by Fe-Containing Particles and Environmental  
720 Implications, *Environ. Sci. Technol.*, 53, 1269-1277, 2019.
- 721 Zhang, H. H., Li, R., Dong, S. W., Wang, F., Zhu, Y. J., Meng, H., Huang, C. P., Ren, Y.,  
722 Wang, X. F., Hu, X. D., Li, T. T., Peng, C., Zhang, G. H., Xue, L. K., Wang, X. M., and Tang,  
723 M. J.: Abundance and Fractional Solubility of Aerosol Iron During Winter at a Coastal City in  
724 Northern China: Similarities and Contrasts Between Fine and Coarse Particles, *J. Geophys.*  
725 *Res.-Atmos.*, 127, e2021JD036070, 2022.
- 726 Zhang, R., Cao, J. J., Tang, Y. R., Arimoto, R., Shen, Z. X., Wu, F., Han, Y. M., Wang,  
727 G. H., Zhang, J. Q., and Li, G. H.: Elemental profiles and signatures of fugitive dusts from  
728 Chinese deserts, *Sci. Total Environ.*, 472, 1121-1129, 2014.
- 729 Zhang, Y. X., Schauer, J. J., Shafer, M. M., Hannigan, M. P., and Dutton, S. J.: Source  
730 apportionment of in vitro reactive oxygen species bioassay activity from atmospheric  
731 particulate matter, *Environ. Sci. Technol.*, 42, 7502-7509, 2008.
- 732 Zhu, Y., Li, W., Wang, Y., Zhang, J., Liu, L., Xu, L., Xu, J., Shi, J., Shao, L., Fu, P.,  
733 Zhang, D., and Shi, Z.: Sources and processes of iron aerosols in a megacity in Eastern China,  
734 *Atmos. Chem. Phys.*, 22, 2191-2202, 2022.
- 735 Zhu, Y. H., Li, W. J., Lin, Q. H., Yuan, Q., Liu, L., Zhang, J., Zhang, Y. X., Shao, L. Y.,  
736 Niu, H. Y., Yang, S. S., and Shi, Z. B.: Iron solubility in fine particles associated with secondary  
737 acidic aerosols in east China, *Environ. Pollut.*, 264, 114769, 2020.
- 738